Global 3-D Land-Ocean-Atmosphere Model for Mercury: Present-Day Versus Preindustrial Cycles and Anthropogenic Enrichment Factors for Deposition

Global 3-D land-ocean-atmosphere model for mercury: Present-day versus preindustrial cycles and anthropogenic enrichment factors for deposition

Noelle E. Selin,[1,2] Daniel J. Jacob,[1] Robert M. Yantosca,[1] Sarah Strode,[3] Lyatt Jaeglé,[3] and Elsie M. Sunderland[4]

Received 20 June 2007; revised 5 November 2007; accepted 18 December 2007; published 7 May 2008.

[1] We develop a mechanistic representation of land-atmosphere cycling in a global 3-D ocean-atmosphere model of mercury (GEOS-Chem). The resulting land-ocean-atmosphere model is used to construct preindustrial and present biogeochemical cycles of mercury, to examine the legacy of past anthropogenic emissions, to map anthropogenic enrichment factors for deposition, and to attribute mercury deposition in the United States. Land emission in the model includes prompt recycling of recently deposited mercury (600 Mg a^{-1} for present day), soil volatilization (550 Mg a^{-1}), and evapotranspiration (550 Mg a^{-1}). The spatial distribution of soil concentrations is derived from local steady state between land emission and deposition in the preindustrial simulation, augmented for the present day by a 15% increase in the soil reservoir distributed following the pattern of anthropogenic deposition. Mercury deposition and hence emission are predicted to be highest in the subtropics. Our atmospheric lifetime of mercury against deposition (0.50 year) is shorter than past estimates because of our accounting of Hg(0) dry deposition, but recycling from surface reservoirs results in an effective lifetime of 1.6 years against transfer to long-lived reservoirs in the soil and deep ocean. Present-day anthropogenic enrichment of mercury deposition exceeds a factor of 5 in continental source regions. We estimate that 68% of the deposition over the United States is anthropogenic, including 20% from North American emissions (20% primary and <1% recycled through surface reservoirs), 31% from emissions outside North America (22% primary and 9% recycled), and 16% from the legacy of anthropogenic mercury accumulated in soils and the deep ocean.

Citation: Selin, N. E., D. J. Jacob, R. M. Yantosca, S. Strode, L. Jaeglé, and E. M. Sunderland (2008), Global 3-D land-ocean-atmosphere model for mercury: Present-day versus preindustrial cycles and anthropogenic enrichment factors for deposition, *Global Biogeochem. Cycles*, *22*, GB2011, doi:10.1029/2007GB003040.

1. Introduction

[2] Efforts to reduce mercury deposition and its impacts on ecosystems have focused on controlling direct anthropogenic emissions from coal combustion, waste incineration, and mining [*Pacyna et al.*, 2006]. However, these emissions amount to only about a third of the global present-day release of mercury to the atmosphere [*Mason and Sheu*, 2002]. Emissions from land and ocean surfaces account for the remainder, but the cycling of mercury in these compartments is not well understood, particularly the rerelease of previously deposited anthropogenic mercury [*Pirrone et al.*, 1996]. We address this issue here with a global 3-D coupled atmosphere-land-ocean model applied to the biogeochemical cycling of mercury for present-day versus pre-industrial conditions.

[3] Our work builds on a previously developed atmosphere-ocean model for mercury based on a global 3-D atmospheric chemical transport model (GEOS-Chem CTM) coupled to a 2-D (horizontal) slab model of the ocean mixed layer [*Strode et al.*, 2007]. The atmospheric component [*Selin et al.*, 2007] simulates the transport and chemical evolution of elemental mercury (Hg(0)), semivolatile oxidized mercury (Hg(II)), and refractory particulate mercury (Hg(P)). The atmosphere is coupled with the ocean through deposition of Hg(II) and Hg(P), two-way exchange of Hg(0), photochemical and biological cycling between Hg(0) and Hg(II) in the ocean mixed layer, and exchange with the subsurface ocean viewed as a fixed reservoir

[1]Department of Earth and Planetary Sciences and School of Engineering and Applied Sciences, Harvard University, Cambridge, Massachusetts, USA.
[2]Now at Joint Program on the Science and Policy of Global Change and Center for Global Change Science, Department of Earth, Atmospheric and Planetary Sciences, Massachusetts Institute of Technology, Cambridge, Massachusetts, USA.
[3]Department of Atmospheric Sciences, University of Washington, Seattle, Washington, USA.
[4]U.S. Environmental Protection Agency, Washington, D.C., USA.

0886-6236/08/2007GB003040$12.00

[*Strode et al.*, 2007]. We present here the addition of a coupled land component to that model, thus fully accounting for the cycling of mercury between the atmosphere and the surface reservoirs of the Earth. Coupling of GEOS-Chem to the deep ocean is being developed in separate work [*Sunderland and Mason*, 2008].

[4] Primary emission of mercury to the land-ocean-atmosphere system involves transfer from the lithosphere. This transfer has a natural component (weathering, volcanoes) and has been augmented by human activity (fossil fuel combustion, waste incineration, mining) [*Mason et al.*, 1994; *Mason and Sheu*, 2002]. The transfer is mostly to the atmosphere as Hg(0), although there is also some Hg(II) and Hg(P) emission from fuel combustion. The lifetime of atmospheric mercury with respect to deposition is estimated at 1.1 ± 0.3 years (see literature review by *Selin et al.* [2007]), with ~60% of deposition taking place to land [*Mason and Sheu*, 2002]. Cycling of deposited mercury in the land reservoir is determined by exchange between vegetation and soil, binding to organic material, Hg(0)/Hg(II) redox chemistry, and Hg(0) volatilization [*Zhang and Lindberg*, 1999].

[5] Several studies have estimated global mercury emission from land by extrapolating the sparse flux measurement data or by imposing mass balance constraints. On the basis of flux measurements in Tennessee and Sweden, *Lindberg et al.* [1998] estimated a land emission between 1400 and 3400 Mg a^{-1}. Using a global box model and observational constraints imposed by the interhemispheric gradient of atmospheric mercury and sediment archives, *Lamborg et al.* [2002] estimated a natural land emission of 1000 Mg a^{-1}. By scaling up measured fluxes from different land types and using constraints imposed by a global mass balance, *Mason and Sheu* [2002] estimated a natural land flux of 800 Mg a^{-1} and an additional 800 Mg a^{-1} from recycling of previously deposited anthropogenic mercury. These estimates of the land source are comparable to the present-day anthropogenic mercury emission, estimated at 2200 Mg a^{-1} [*Pacyna et al.*, 2006].

[6] A global 3-D atmospheric CTM including Hg(0)/Hg(II) redox chemistry is essential for modeling land-atmosphere exchange of mercury since deposition is mostly as short-lived Hg(II). However, previous global atmospheric CTMs have not attempted to enforce consistency between atmospheric deposition and land emission. *Shia et al.* [1999] used a land source of 2000 Mg a^{-1} uniformly distributed over land with no temporal variation. *Bergan et al.* [1999] and *Seigneur et al.* [2001] distinguished between primary (nonrecycled) emissions (500 Mg a^{-1}) distributed over areas of geological deposits, and re-emission of previously deposited mercury (1500–2000 Mg a^{-1}) distributed according to present-day deposition patterns. More mechanistically based parameterizations of land-atmosphere exchange have been developed for regional models in North America [*Xu et al.*, 1999, 2000; *Bash et al.*, 2004; *Lin et al.*, 2005; *Gbor et al.*, 2006], but even these have made little effort to relate local deposition to land emission.

[7] We develop here a simple mass balanced, mechanistically based representation of land-atmosphere exchange of mercury for global models and apply it to the GEOS-Chem CTM. We first conduct a steady state preindustrial simulation for mercury to constrain the magnitude and spatial variability of natural land emissions. We then construct the perturbed global biogeochemical cycle for present-day conditions including the added input from anthropogenic emissions. We derive global budgets and lifetimes, estimate anthropogenic enrichment factors for deposition in different parts of the world, and assess the legacy of anthropogenic influence from re-emission of previously deposited mercury.

2. Ocean-Atmosphere Model

[8] The ocean-atmosphere version of the model has been previously described by *Selin et al.* [2007] and *Strode et al.* [2007]. We give here a brief summary of the original model and elaborate on recent updates. Implementation of land-atmosphere cycling will be described in section 3.

2.1. Original Model

[9] The original GEOS-Chem atmosphere-ocean model is described by *Selin et al.* [2007] for the atmosphere and by *Strode et al.* [2007] for the ocean. The simulation is based on GEOS-Chem version 7.04 (http://www.as.harvard.edu/chemistry/trop/geos/) [*Bey et al.*, 2001]. It includes three transported species in the atmosphere: elemental mercury (Hg(0)), semivolatile divalent mercury (Hg(II)), and refractory particulate mercury (Hg(P)). GEOS-Chem uses assimilated meteorological data from the NASA Goddard Earth Observing System (GEOS-4), including winds, mixed layer depths, temperature, precipitation, and convective mass fluxes. These data are available with 6-hour temporal resolution (3-hour for surface quantities and mixing depths), a horizontal resolution of 1° × 1.25°, and 55 hybrid sigma-pressure levels in the vertical. The horizontal resolution is degraded here to 4° × 5° for input to GEOS-Chem. Simulations are conducted for a 6-year period (2000–2005), with the first 3 years used for initialization. The ocean simulation is a slab model for the ocean mixed layer with the same horizontal resolution as the atmospheric simulation. It includes three species in the aqueous phase: Hg(0), Hg(II), and nonreactive Hg. Horizontal transport in the ocean is neglected. Each ocean box communicates with the atmospheric box directly above and with a subsurface ocean containing uniform mercury concentrations.

[10] The GEOS-Chem atmospheric simulation described by *Selin et al.* [2007] uses the 2000 GEIA global emissions inventory for anthropogenic sources of Hg(0), Hg(II), and Hg(P) (1278, 720, and 192 Mg a^{-1} respectively) [*Pacyna et al.*, 2006]. Ocean-atmosphere exchange of Hg(0) and Hg(II) is simulated with a standard two-layer model. Emissions from land are described further below. Atmospheric redox chemistry includes oxidation of Hg(0) to Hg(II) by OH ($k = 9 \times 10^{-14}$ cm^3 s^{-1} [*Sommar et al.*, 2001; *Pal and Ariya*, 2004]) and ozone ($k = 3 \times 10^{-20}$ cm^3 s^{-1} [*Hall*, 1995]). It also includes in-cloud first-order photochemical reduction of Hg(II) to Hg(0) ($k = 8.4 \times 10^{-10}[OH]_g$ s^{-1}, where $[OH]_g$ is the gas-phase OH concentration in molecules cm^{-3}) scaled to match constraints on the observed seasonal variation and interhemispheric gradient of total

gaseous mercury (TGM ≡ Hg(0) + Hg(II)). OH and O_3 concentrations are monthly mean 3-D fields from a detailed GEOS-Chem tropospheric chemistry simulation [*Park et al.*, 2004]. *Holmes et al.* [2006] suggested that Br could be a major Hg(0) photochemical oxidant, possibly more important than OH, but from our standpoint the exact mechanism for Hg(0)/Hg(II) redox cycling of is of little consequence since rate constants are adjusted to match observational constraints. Hg(P) is viewed as chemically inert, consistent with its operational definition in the GEIA inventory. Hg(II) can partition between gas and particulate phases but the mechanism is uncertain; this partitioning matters here only in the deposition calculation, for the purpose of which we view Hg(II) as a water-soluble gas. Hg(II) and Hg(P) are removed by dry deposition with a standard resistance-in-series scheme [*Wesely*, 1989; *Wang et al.*, 1998] and by wet deposition with a scheme including convective and large-scale rainout and washout, as well as scavenging in wet convective updrafts [*Liu et al.*, 2001]. Zero-retention efficiency is assumed for Hg(II) when clouds freeze below 268 K. Dry deposition of Hg(0) to the oceans is simulated as part of the bidirectional exchange model of *Strode et al.* [2007].

[11] The GEOS-Chem ocean simulation described by *Strode et al.* [2007] deposits Hg(II) to the ocean as $Hg(II)_{(aq)}$, where it is reduced to $Hg(0)_{(aq)}$ at a rate proportional to solar radiation and net primary productivity (NPP), and taken up by particles as nonreactive Hg at a rate proportional to NPP. Deposited Hg(P) enters the nonreactive pool. $Hg(0)_{(aq)}$ exchanges with atmospheric Hg(0) as determined by its temperature-dependent Henry's law constant [*Wängberg et al.*, 2001] and a wind-dependent gas exchange velocity [*Nightingale et al.*, 2000]. Nonreactive Hg sinks to the deeper ocean at a rate determined by the organic carbon flux (biological pump). All three species also exchange with the subsurface ocean via upwelling, downwelling, and diffusion across the thermocline. Subsurface ocean concentrations are fixed at 0.06 pM $Hg(0)_{(aq)}$, 0.5 pM $Hg(II)_{(aq)}$, and 0.5 pM nonreactive Hg as means of present-day values. Land Hg(0) emissions described by *Selin et al.* [2007] include (1) a geogenic source of 500 Mg a^{-1} [*Lindqvist*, 1991] distributed according to the locations of mercury mines (D. G. Frank, Mineral Resource Data System (MRDS) data in Arc View shape file format, for spatial data delivery project, 1999, U.S. Geological Survey, Spokane, Washington, available athttp://webgis.wr.usgs.gov/globalgis/metadata_qr/ore_deposits_qk_ref.htm) as an indicator of mercury deposits and (2) a re-emission source of 1500 Mg a^{-1} distributed according to the patterns of present-day sources, following the methodology of *Bergan et al.* [1999] and *Seigneur et al.* [2001]. The geogenic source represents mobilization of mercury by degassing from geological reservoirs and is taken to account for volcanic activity. Independent emission estimates from volcanoes are in the 45–700 Mg a^{-1} range [*Fitzgerald and Lamborg*, 2005; *Nriagu and Becker*, 2003; *Pyle and Mather*, 2003]. The re-emission source represents recycling from the land mercury pool supplied by atmospheric deposition [*Schlüter*, 2000]. A focus of the present work is to improve this land component both on a process level and in a manner that provides consistency in the biogeochemical cycling of mercury. This will be discussed in section 3.

2.2. Model Updates

[12] For this work, we improved the atmospheric simulation of *Selin et al.* [2007] to include dry deposition of Hg(0) to land as well as additional emissions from biomass burning and artisanal mining. Uptake of Hg(0) by vegetation is thought to occur at the leaf interior, and is thus controlled by gas exchange at the stomata [*Lindberg et al.*, 1992]. *Poissant et al.* [2004] measured Hg(0) dry deposition velocities as high as 0.19 cm s^{-1} over wetland vegetation; *Lindberg et al.* [2002] report a midday mean velocity of 0.14 ± 0.13 cm s^{-1} over a cattail stand in the Florida Everglades. *Lindberg et al.* [1992] estimated dry deposition velocities to a deciduous forest of 0.12 cm s^{-1} in summer and 0.006 cm s^{-1} in winter on the basis of measured mesophyll resistances [*Du and Fang*, 1982]. Following *Lin et al.* [2006], we describe Hg(0) dry deposition with the standard *Wesely* [1989] resistance-in-series scheme as a function of the Henry's law constant (0.11 M atm^{-1} [*Lin and Pehkonen*, 1999]) and a "reactivity factor" f_o of 10^{-5} to match the above observations. The resulting annual mean dry deposition velocity to all land types is 0.03 cm s^{-1}, with values over the continental United States in July exceeding 0.14 cm s^{-1} in daytime. This leads in the model to a present-day dry deposition sink of Hg(0) to land of 1600 Mg a^{-1}. Dry deposition of Hg(0) to the ocean is an additional sink of 2200 Mg a^{-1}. In comparison, *Selin et al.* [2007] derived a mercury deposition sink of 7000 Mg a^{-1} accounting only for Hg(II) and Hg(P). Accounting for Hg(0) deposition in our updated model yields an atmospheric lifetime for TGM of 0.50 year, as compared to 0.79 year in the work of *Selin et al.* [2007] and a literature range of 0.71–1.7 years reviewed in that paper. These previous studies did not explicitly account for Hg(0) deposition to the ocean (the ocean was simply treated as a net source) and either ignored Hg(0) deposition to land or used a prescribed slow deposition velocity. As we will see, a 0.50 year lifetime for TGM is not inconsistent with the constraints from atmospheric observations.

[13] Global emissions from biomass burning are estimated at 100–860 Mg a^{-1} on the basis of extrapolations of field and laboratory data from different ecosystem types [*Friedli et al.*, 2003]. Measurements of Hg/CO correlations in biomass burning plumes indicate molar emission ratios ranging from 0.67 to 2.1 × 10^{-7} [*Andreae and Merlet*, 2001; *Brunke et al.*, 2001; *Friedli et al.*, 2001, 2003; *Ebinghaus et al.*, 2007]. Areas with high mercury concentrations such as peatlands may have higher emission ratios, but *Turetsky et al.* [2006] estimate that they contribute only 20 Mg a^{-1} to global mercury emissions. We adopt an Hg/CO emission ratio of 2.1 × 10^{-7} and apply it to a monthly gridded climatological inventory of biomass burning CO emissions (437 Tg CO a^{-1}) [*Duncan et al.*, 2003]. We thus obtain a spatially and temporally resolved distribution of mercury emissions from biomass burning with a global total of 600 Mg a^{-1}, and assume that all emission is as Hg(0).

[14] Artisanal mining is not included in the GEIA anthropogenic emission inventory of *Pacyna et al.* [2006].

Hylander and Meili [2005] estimated the artisanal mining use of mercury by country for 2000. We use their means for each country, assume that 75% is emitted to the atmosphere (all as Hg(0)), consistent with 25% removal to mine tailings [*Wong et al.*, 1999], and spatially distribute emissions evenly over the country. The resulting global emission is 450 Mg a^{-1}. A study by *Swain et al.* [2007] estimated a somewhat smaller artisanal mining emission (300 Mg a^{-1}) though higher total mercury use (1000 Mg a^{-1}). Most of the artisanal mining source is in Asia (200 Mg a^{-1}), with China (188 Mg a^{-1}) contributing the majority. Africa emits 35 Mg a^{-1}, the Americas 94 Mg a^{-1}, and the former Soviet Union countries 15 Mg a^{-1}. This represents a substantial addition to the GEIA global anthropogenic Hg(0) emission of 1278 Mg a^{-1} from *Pacyna et al.* [2006].

[15] We further increase the Asian Hg(0) anthropogenic source inventory from *Pacyna et al.* [2006] by 50% to account for the regional underestimate identified by *Jaffe et al.* [2005] from CO-Hg(0) correlation measurements in Chinese outflow. This represents an additional 330 Mg a^{-1} added to the inventory. The total Hg(0) emission from all sources in East Asia in GEOS-Chem (17–50°N, 75–135°E) is now 1460 Mg, consistent with the estimate of *Jaffe et al.* [2005].

[16] The previous GEOS-Chem simulation of *Selin et al.* [2007] using a global source of 7000 Mg a^{-1} was globally unbiased when compared to TGM observations at land-based sites. Inclusion in the present simulation of the Hg(0) first-order sink from dry deposition (1600 Mg a^{-1}) requires compensating additional sources to avoid a low bias. Inclusion of the biomass burning and artisanal mining emissions, and augmentation of Chinese anthropogenic emissions, add a total of 1400 Mg a^{-1}. We need an additional 300 Mg a^{-1}. This is within the uncertainty bound reported for the inventory of *Pacyna et al.* [2006], which may be underestimated in part owing to its stated under-accounting of waste incineration. Thus we assume that anthropogenic emissions outside Asia in the GEIA inventory (totaling 1011 Mg a^{-1}) are uniformly too low by 30% for all three Hg species.

3. Land-Atmosphere Cycling

[17] Transfer of mercury from the atmosphere to the land reservoir takes place by dry deposition of Hg(0) and by wet and dry deposition of Hg(II) and Hg(P). A fraction of deposited Hg(II) is quickly converted to Hg(0) and re-emitted, a process which we term "prompt recycling." The remainder is transferred to the soil by throughfall and litterfall and enters the longer-lived soil pool where it partitions between the solid and aqueous phases, undergoes redox chemistry, and eventually (on a millennial timescale) returns to the atmosphere as Hg(0) through evapotranspiration and volatilization. The observational basis for these processes and their implementation in GEOS-Chem are discussed in the following subsections.

3.1. Soil Mercury Pool

[18] Soil mercury is dominated by the solid-phase pool, which is mainly Hg(II) bound to soil organic matter [*Ravichandran*, 2004]. We consider as relevant soil reservoir in our analysis the layer ~15 cm deep where mercury has a residence time of 100–1000 years against evasion to the atmosphere [*Andren and Nriagu*, 1979; *Grigal*, 2003]. Estimates of the global mean mercury concentration in that pool are extremely limited, but available estimates vary from 20 to 70 ng g^{-1} [*Andersson*, 1967; *Shacklette et al.*, 1971; *Richardson et al.*, 2003; *Frescholtz and Gustin*, 2004]. We assume here a global average solid soil concentration $\bar{C}_s$ of 50 ng g^{-1} for the present day and 43 ng g^{-1} for pre-industrial conditions, on the basis of the estimate of *Mason and Sheu* [2002] that anthropogenic activities have increased the soil mercury pool by 15%. Using a 15 cm soil depth and a soil density of 1.3 g cm^3 [*Hillel*, 1998], we thus estimate a preindustrial solid soil mercury pool of 1×10^6 Mg. The corresponding present-day value is 1.15×10^6 Mg.

[19] We determine the spatial variability of soil concentrations by assuming that each 4° × 5° model land grid square is in yearly steady state in our preindustrial simulation; that is, total annual deposition in the grid square (dry and wet deposition of Hg(II) plus dry deposition of Hg(0)) is equal to total annual emission (volatilization from solid soil, evapotranspiration, and prompt recycling). Hg(P) is 100% anthropogenic and thus is not included in the preindustrial simulation. We neglect runoff, which amounts to only 40 Mg a^{-1} in the global preindustrial budget of *Mason and Sheu* [2002], and we do not include the geogenic source as part of the steady state constraint. The local solid soil concentration C_s used to calculate evapotranspiration and volatilization (equations (2) and (3) below) is related to the global mean value $\bar{C}_s$ (43 ng g^{-1} for preindustrial, 50 ng g^{-1} for present day) by

$$C_s(x,y) = A(x,y)\bar{C}_s, \quad (1)$$

where the spatial scaling factor $A(x,y)$ is determined iteratively by starting from a uniform field $A(x,y) = 1$, conducting 1 year of preindustrial simulation, locally adjusting $A(x,y)$ for steady state, and repeating over successive years until convergence. Achieving convergence within 5% for all 4° × 5° land boxes requires 5 years of simulation. For the present-day land, we adjust $A(x,y)$ by distributing the 15% global increase in soil concentration following the present-day anthropogenic deposition pattern.

3.2. Prompt Recycling

[20] Isotopic field studies [*Hintelmann et al.*, 2002; *Graydon et al.*, 2006] have shown that newly deposited mercury behaves differently than the strongly bound mercury resident in soil and vegetation. Newly deposited mercury is more available for emission on a timescale of days to months after deposition, beyond which it becomes indistinguishable from the resident mercury. Empirical estimates of this prompt recycling range from 5 to 40% of deposited Hg(II) [*Hintelmann et al.*, 2002; *Amyot et al.*, 2004], increasing to 60% for surface snow [*Lalonde et al.*, 2001; *Ferrari et al.*, 2005]. We implement prompt recycling in the model by returning 20% of wet and dry deposited Hg(II) to the atmosphere as Hg(0) immediately upon deposition to land (60% for snow covered land, based on local GEOS-4 snow cover information). Prompt recycling of Hg(II)

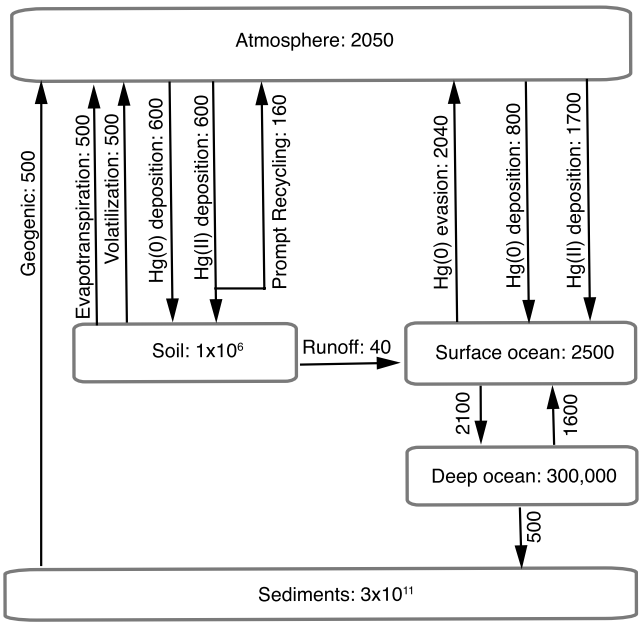

Figure 1. Global preindustrial biogeochemical cycle of mercury in GEOS-Chem. Inventories are in Mg and rates are in Mg a^{-1}. All reservoirs are in steady state.

deposition corresponds to a land source of 600 Mg a^{-1} in the present-day budget and 160 Mg a^{-1} in the preindustrial budget.

3.3. Evapotranspiration

[21] Evapotranspiration mobilizes mercury in soil water to the atmosphere, both through vegetation and directly from the soil. Following *Xu et al.* [1999], we calculate the evapotranspirative mercury emission flux per unit area of Earth surface (F_e, ng m^{-2} s^{-1}) as the product of the soil water mercury concentration and the water evapotranspiration rate (E, mm s^{-1}). The soil water mercury concentration is related to the solid soil mercury concentration (C_s, ng g^{-1}) by the soil-water partition coefficient K_d = 6310 L kg^{-1} [*Allison and Allison*, 2005], so that

$$F_e = EC_s/K_d. \tag{2}$$

[22] We obtain E_c from gridded 4° × 5° monthly mean climatological evapotranspiration fields [*Mintz and Walker*, 1993]. The global mean evapotranspiration rate is 0.8 mm d^{-1}, and the resulting evapotranspiration source is 500 Mg a^{-1} in the preindustrial simulation and 550 Mg a^{-1} in the present-day simulation.

3.4. Soil Volatilization

[23] Hg(0) volatilization from the solid soil pool depends on both temperature [*Kim et al.*, 1995; *Lindberg et al.*, 1995] and solar radiation [*Carpi and Lindberg*, 1998; *Gustin et al.*, 2002]. Soil moisture also affects volatilization but apparently only in very dry soils (moisture level < 15 vol% [*Gustin and Stamenkovic*, 2005]). We calculate the local Hg(0) volatilization flux F_v (ng m^{-2} h^{-1}) by compounding the solar radiation dependence from *Zhang et al.* [2001] and the temperature dependence from *Poissant and Casimir* [1998]:

$$F_v = \beta C_s \exp\left[-1.1 \times 10^4/T\right] \exp\left[1.1 \times 10^{-3} R_g\right], \tag{3}$$

where R_g is the solar radiation flux at the ground (W m^{-2}) and T is the surface skin temperature (K). The preexponential factor β = 1.5 × 10^{15} ng m^{-2} h^{-1} constrains the global magnitude of emissions by mass balance in the preindustrial budget, as described in section 4. Surface skin temperature and solar radiation at canopy top (R_S) are available locally from the GEOS-4 archive. R_g is derived from R_S by allowing for light attenuation by the canopy:

$$R_g = R_s \exp[-\alpha L/\cos\theta], \tag{4}$$

where L is the monthly mean leaf area index of the canopy derived from AVHRR satellite data [*Myneni et al.*, 1997], θ is the solar zenith angle, and α = 0.5 is an extinction coefficient assuming random angular distribution of leaves [*Verstraete*, 1987]. The global soil volatilization source is 500 Mg a^{-1} in the preindustrial simulation and 550 Mg a^{-1} in the present-day simulation, similar in magnitude to the evapotranspirative source but with different spatial distribution as will be discussed in section 4.2.

4. Preindustrial Mercury Cycle

4.1. Global Budget

[24] Figure 1 shows the global preindustrial biogeochemical cycle of mercury in GEOS-Chem. We view "preindustrial" as describing steady state natural conditions, although emissions from mining activity prior to the industrial revolution may not have been negligible [*Roos-Barraclough et al.*, 2002]. We also assume that first-order processes involving atmospheric and ocean mixed layer concentrations have the same rate constants in the preindustrial and present atmospheres, and we use the same oxidant fields. This enables simple scalings between the present-day and preindustrial budgets. Changes in OH, the main Hg(0) oxidant in our simulation, have likely been less than 10% from preindustrial to present [*Wang and Jacob*, 1998].

[25] A central constraint in our construction of the preindustrial cycle is evidence from sediment core data that present-day global deposition of mercury is enriched by a factor of three above preindustrial [*Mason and Sheu*, 2002]. A review by *Fitzgerald et al.* [1998] reports a mean enrichment ratio of 2.7 ± 0.9 for 40 U.S. and Canadian lakes, and 2.0–2.6 for Scandinavia; higher ratios are found near anthropogenic sources. The present-day mercury deposition in GEOS-Chem is 11,200 Mg a^{-1} and hence we impose the preindustrial deposition to be 3700 Mg a^{-1}. Because deposition from anthropogenic emissions of Hg(II) and Hg(P) is small on the global scale, the constraint on deposition implies that the preindustrial atmospheric inventory of mercury in the atmosphere is also one third of the present-day value of 5600 Mg and hence 1970 Mg. Finally, the steady state assumption for the preindustrial cycle requires that total emissions be equal

to deposition (3700 Mg a^{-1}). We also assume ocean concentrations immediately below the mixed layer to be one-third the present-day levels given by *Strode et al.* [2007], consistent with the deposition constraint.

[26] The preindustrial simulation includes no anthropogenic emissions, and biomass burning emissions are assumed negligible. As in the present-day simulation [*Selin et al.*, 2007] and described in section 2.1, mercury is mobilized from geogenic sources to the atmosphere through weathering and degassing at a rate of 500 Mg a^{-1}. This provides the primary source to the land-ocean-atmosphere pool and is balanced by return of mercury to the deep-ocean sediments.

[27] Deep ocean, soil, and sediment reservoirs are not explicitly simulated in GEOS-Chem but are included in the global biogeochemical cycle of Figure 1. The soil pool is estimated as given in section 3.2. The preindustrial deep ocean pool is estimated to be 300,000 Mg [*Sunderland and Mason*, 2008] and the sediment pool 3×10^{11} Mg [*Andren and Nriagu* [1979]. Runoff processes are neglected in our model simulation, but we include the 40 Mg a^{-1} estimate of *Mason et al.* [1994] in our preindustrial budget of Figure 1 for the sake of completeness.

[28] We derive the preindustrial soil volatilization source by mass balance in the steady state global preindustrial budget. As specified by the global deposition constraint, the total preindustrial mercury emission must be 3700 Mg a^{-1}. We specify as noted above a global geogenic emission total of 500 Mg a^{-1}. Using the slab model of *Strode et al.* [2007], with deep ocean concentrations a factor of three lower than the present day, we obtain an oceanic Hg(0) emission of 2040 Mg a^{-1}. The evapotranspirative emission is 500 Mg a^{-1} (section 3.3). The prompt recycling source from Hg(II) deposition is 160 Mg a^{-1} (section 3.1). Steady state then implies a soil volatilization source of 500 Mg a^{-1} (total deposition of 3700 Mg a^{-1}, minus all other emissions amounting to 3200 Mg a^{-1}). We choose the scaling factor β in our soil volatilization parameterization of equation (3) to enforce this constraint.

[29] Mercury deposition fluxes are obtained from the GEOS-Chem simulation with the sources specified above. All emission in the preindustrial simulation is as Hg(0), which has a sufficiently long lifetime to mix globally in the atmosphere. Thus 68% of deposition in GEOS-Chem is to ocean (2500 Mg a^{-1}), and 32% is to land (1200 Mg a^{-1}). Total Hg(II) deposition to land is 600 Mg a^{-1}, of which 180 Mg a^{-1} is wet and 420 Mg a^{-1} is dry. Dry deposition of Hg(0) to land is 600 Mg a^{-1}. The net Hg(0) flux out of the ocean is 1240 Mg a^{-1}, which represents a balance between gross fluxes of Hg(0) dry deposition (800 Mg a^{-1}) and evasion (2040 Mg a^{-1}). Exchange between the ocean mixed layer and the deep ocean [*Strode et al.*, 2007] results in a downwelling flux of 2100 Mg a^{-1} out of the mixed layer, partly balanced by an upwelling flux of 1600 Mg a^{-1}. The ocean is thus a net sink of 500 Mg a^{-1} for atmospheric mercury, balancing the geogenic source.

[30] We find from Figure 1 that the overall lifetime of mercury in the combined atmosphere-ocean-terrestrial system against transfer to the sediments is about 3000 y. This is shorter than 10,000 years in the budget of *Mason and Sheu* [2002], where the burial rate was lower because the estimated geogenic source was lower. It is considerably shorter than the corresponding lifetime of carbon ($\sim 2 \times 10^5$ years [*McElroy*, 2002]), which may be explained by preferential partitioning of oceanic mercury to precipitable organic matter.

[31] Mercury in the model has a relatively short lifetime in the atmosphere (0.55 y) and in the surface ocean (0.60 y), while its lifetime in soils is much longer (1000 y). We find that while 50% of the mercury deposited to the oceans returns to the atmosphere as opposed to sinking to the deep ocean, only a smaller fraction (10%) of mercury deposited to land is similarly recycled to the atmosphere on short timescales (through the prompt recycling mechanism applied to Hg(II) deposition). As a result, we find that geogenic Hg(0) emitted to the atmosphere is transferred to the soil and the deep ocean reservoirs in equal amounts, even though deposition to the ocean is twice as large.

4.2. Spatial Distribution of Surface Fluxes

[32] Figure 2 shows the spatial distributions of mercury deposition fluxes in the preindustrial simulation from Hg(0) dry deposition, Hg(II) dry deposition, and Hg(II) wet deposition; also shown is the concentration of Hg(II) at 800 hPa. Deposition of Hg(0) to land largely follows the leaf area index pattern. Deposition of Hg(0) to the ocean (gross flux) is highest for low temperatures (high Hg(0) solubility) and high winds. Dry deposition of Hg(II) is highest in the subtropics, reflecting high boundary layer concentrations of Hg(II) (Figure 2d) brought down by subsidence in the general circulation [*Selin et al.*, 2007]. Wet deposition of Hg(II) is highest where this global-scale subtropical downwelling interacts with regional circulation regimes promoting precipitation, such as in the southeast United States.

[33] Figure 3 shows the spatial patterns of total mercury deposition and of the different source terms (soil volatilization, evapotranspiration, prompt recycling, geogenic emission, ocean evasion) in the preindustrial GEOS-Chem simulation. Geogenic emission follows the locations of the global mercuriferous belts where mercury is geologically enriched. Oceanic evasion is high in areas of high temperature, wind speed, and aqueous Hg(0) concentrations, showing similar patterns to those reported by *Strode et al.* [2007]. Land emission is highest where deposition is highest, reflecting the steady state assumption.

5. Present-Day Mercury Cycle

5.1. Global Budget

[34] Figure 4 shows the present-day global biogeochemical cycle of mercury in GEOS-Chem. Compared with previous estimates, we have a larger primary anthropogenic source (3400 Mg a^{-1} versus 2460 ± 650 Mg a^{-1} in the literature) and a larger total mercury source (11,200 Mg versus 6200 ± 830 Mg a^{-1}) [*Selin et al.*, 2007]. Our larger anthropogenic source reflects the inclusion of emissions from biomass burning and artisanal mining, revised emission estimates from Asia, and global upward adjustment of the GEIA anthropogenic emission inventory (section 2.2).

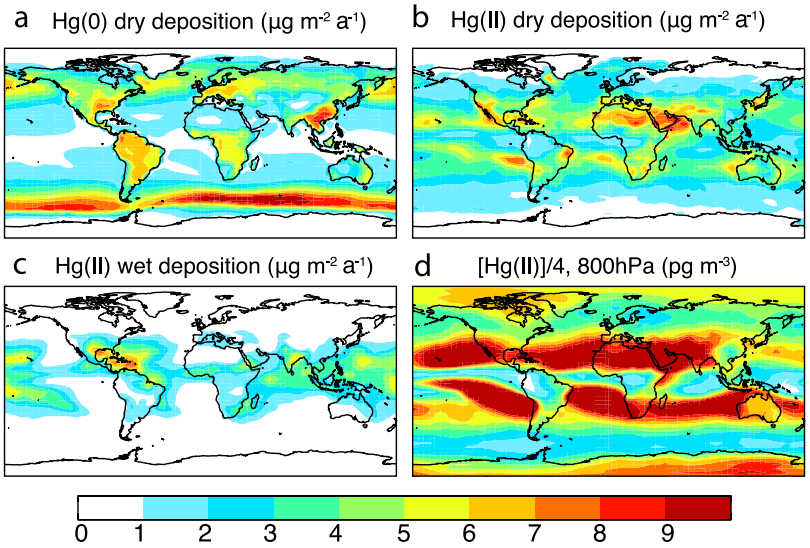

Figure 2. Annual mean deposition fluxes in the preindustrial simulation: (a) Hg(0) dry deposition, (b) Hg(II) dry deposition, and (c) Hg(II) wet deposition (μg m^{-2} a^{-1}). (d) Annual mean Hg(II) concentrations at 800 hPa (pg m^{-3}) divided by 4.

Beyond this anthropogenic source, our larger total source mainly reflects our separate accounting of Hg(0) dry deposition and evasion from the ocean (2200 Mg a^{-1} and 5000 Mg a^{-1}, respectively), rather than the net evasion term reported by previous models.

[35] Our total primary anthropogenic emission is 3400 Mg a^{-1} (2300 Mg a^{-1} as Hg(0), 940 Mg a^{-1} as Hg(II), and 250 Mg a^{-1} as Hg(P)), including 450 Mg a^{-1} from artisanal mining. Emissions from evapotranspiration and soil volatilization are 550 Mg a^{-1} each. Prompt recycling releases 600 Mg a^{-1}, and 600 Mg a^{-1} is emitted from biomass burning. The estimate of runoff is from *Mason and Sheu* [2002] and is increased by a factor of 5 from the preindustrial owing to increases in deposition and effluent release. The deep ocean mercury pool is increased by 17% relative to preindustrial [*Sunderland and Mason*, 2008], and we assume a corresponding enrichment in burial to 600 Mg a^{-1}. The 0.5×10^5 and 1.5×10^5 Mg respective increases in the deep ocean and soil reservoirs since preindustrial times are consistent with the estimate of *Mason et al.* [1994] that 2×10^5 Mg of mercury have been emitted to the atmosphere-land-ocean system since industrialization.

[36] The atmosphere and surface ocean mixed layer are in steady state in the present-day simulation because of their short lifetimes (<1 y). The longer-lived reservoirs (soil and deep ocean) are not in steady state. The lifetime of the soil

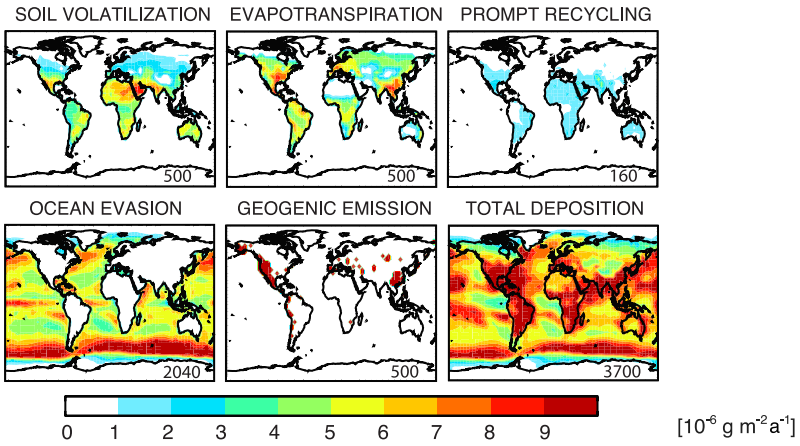

Figure 3. Annual mean surface fluxes in the preindustrial simulation: soil volatilization, evapotranspiration, prompt recycling, ocean evasion, geogenic emission, and total deposition (μg m^{-2} a^{-1}). The total emission from the first five terms equals the deposition flux. Color scale is saturated at the highest levels in the figure. Global totals (Mg a^{-1}) are indicated for each category in the bottom right corner of the panel.

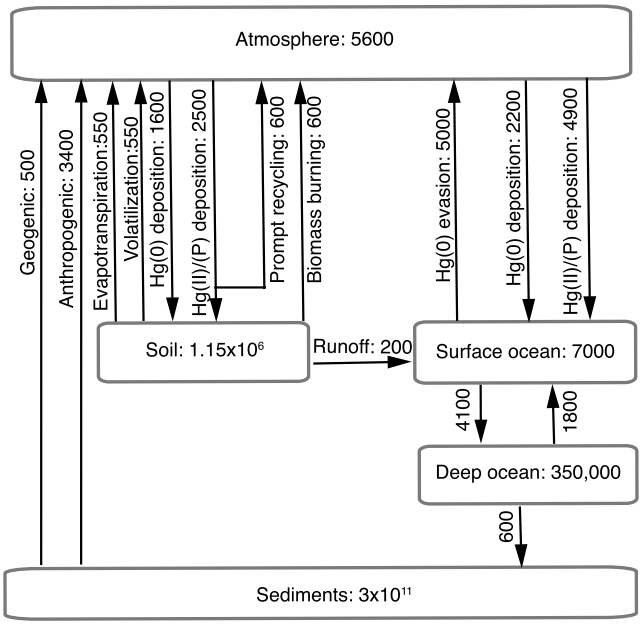

Figure 4. Global present-day biogeochemical cycle of mercury in GEOS-Chem. Inventories are in Mg, and rates are in Mg a^{-1}.

reservoir (10^3 y) implies that perturbations to this reservoir will remain for millennia. In the present-day simulation, the soil reservoir is increasing by 2200 Mg a^{-1} (0.2%). Because the soil reservoir has such a large natural loading, anthropogenic activities have increased its magnitude by only 15%, whereas the deposition flux has increased by a factor of 3.

[37] While the soil reservoir has a very long lifetime, the surface ocean has a much shorter lifetime against re-emission to the atmosphere (1.4 y), implying significant recycling. The subsurface ocean is accumulating 1700 Mg a^{-1} (0.5% a^{-1}) in the present-day simulation. A more detailed accounting of decadal to century-scale perturbations of the ocean cycle, including subsurface and intermediate ocean dynamics, is presented by *Sunderland and Mason* [2008].

5.2. Comparison With Atmospheric Observations

[38] *Selin et al.* [2007] presented comparisons of their GEOS-Chem global mercury simulation with a large ensemble of atmospheric observations. We revisit here these comparisons in terms of the changes made to the model (updates from section 2.2 and section 3). Figure 5 shows the global distribution of TGM ≡ Hg(0) + Hg(II)(g) atmospheric concentrations in our present-day simulation, compared with observations from 22 land sites and from ocean cruises. We have assumed in this comparison as in that of *Selin et al.* [2007] that all Hg(II) in the model is in the gas phase. The model reproduces the mean annual concentration of TGM at the land sites as well as in that of *Selin et al.* [2007] (1.58 ± 0.19 ng m^{-3} measured, 1.56 ± 0.09 ng m^{-3} simulated here, and 1.63 ± 0.10 ng m^{-3} in the work of *Selin et al.* [2007]). As in the work of *Selin et al.* [2007], the simulation is biased low relative to cruise data in the North Atlantic and North Pacific; the cause for this is not clear but might reflect mercury accumulation in the subsurface ocean

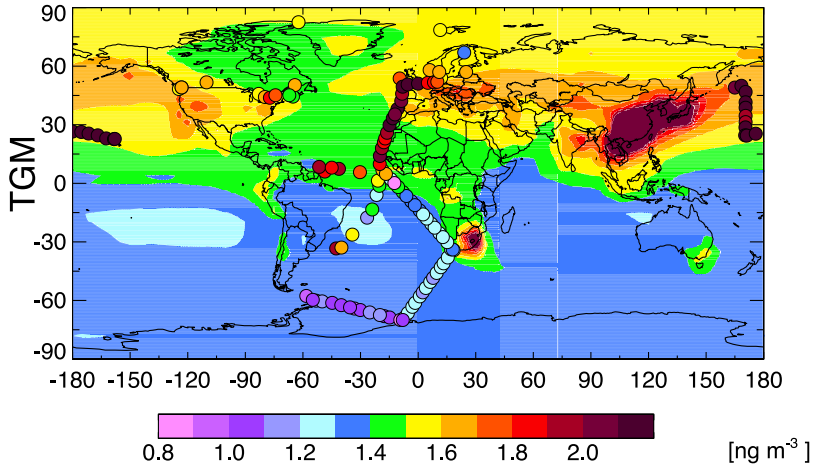

Figure 5. Annual average total gaseous mercury (TGM) concentrations in surface air. Model results (background, for year 2004) are compared to observations (circles) from long-term surface sites [*Baker et al.*, 2002; *Ebinghaus et al.*, 2002; *EMEP*, 2005; *Kellerhals et al.*, 2003; *Poissant et al.*, 2005; *Weiss-Penzias et al.*, 2003; Environment Canada, Canadian Atmospheric Mercury Network, Data, Meterological Service of Canada, Toronto (data set, 2003, not available on internet); Co-operative Programme for Monitoring and Evaluation of the Long-Range Transmissions of Air Pollutants in Europe (EMEP), EMEP measurement data, edited data set, 2005, available at http://www.emep.int/index_data.html] and ship cruises in the Atlantic [*Lamborg et al.*, 1999; *Temme et al.*, 2003] and Pacific [*Laurier et al.*, 2003]. The color scale is the same as that in Figure 2 of *Selin et al.* [2007] and is saturated at the maximum values indicated in the legend.

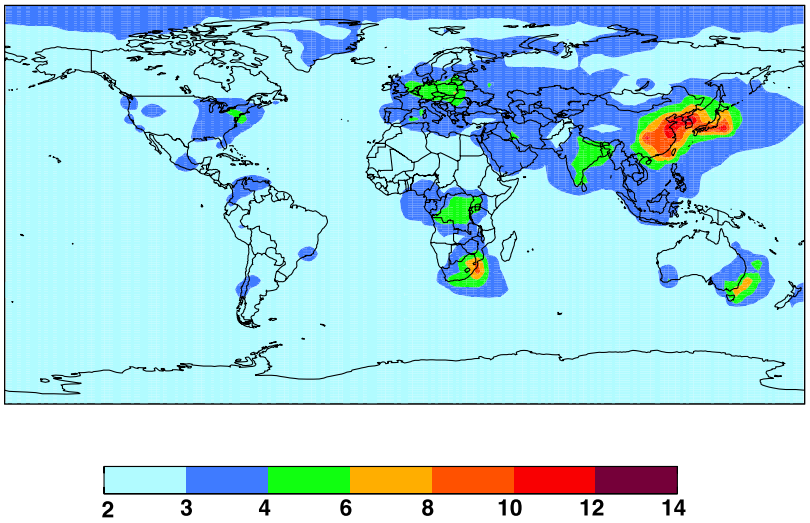

Figure 6. Enrichment factor of present-day relative to preindustrial mercury deposition.

as legacy of mercury emissions over past decades. The vertical distribution of Hg(0) and Hg(II) in the present-day simulation is unchanged relative to that of *Selin et al.* [2007] and is consistent with the few aircraft and mountaintop observations available. The TGM interhemispheric ratio in surface air is 1.2, unchanged relative to that of *Selin et al.* [2007]; the observed ratio is in the range 1.2–1.8 [*Lamborg et al.*, 2002].

[39] The model reproduces well the spatial variation in the annual mean wet deposition fluxes measured by the U.S. Mercury Deposition Network (MDN) (National Atmospheric Deposition Program, Illinois State Water Survey, Champaign, 2003, http://nadp.sws.uiuc.edu/mdn/) (r^2 = 0.60 for 2003–2004, compared with r^2 = 0.69 in the work of *Selin et al.* [2007]). The simulated total wet deposition over the United States is within 16% of that measured by MDN (within 10% of that measured by *Selin et al.* [2007]). Dry deposition data are not collected systematically for mercury, though GEOS-Chem predicts that it should dominate over wet deposition.

[40] Our updated simulation includes increased Hg(0) anthropogenic emission in Asia relative to the GEIA estimate used by *Selin et al.* [2007], to improve consistency with the Hg/CO enhancement ratio measurements of *Jaffe et al.* [2005] at Okinawa, Japan, in April–May 2004. The Hg/CO enhancement ratio for Okinawa determined from the slope of the reduced major axis regression line is 0.0048 ng m^{-3} $ppbv^{-1}$ in the present simulation, as compared to 0.0057 in the data of *Jaffe et al.* [2005] and 0.0039 in the simulation of *Selin et al.* [2007]. *Strode et al.*, [2008] also show that a 50% increase in Asian anthropogenic sources in GEOS-Chem improves this ratio.

[41] *Selin et al.* [2007] also compared the simulated versus observed seasonal variation of TGM at an ensemble of 12 land sites at northern midlatitudes. The measurements show a weak but statistically significant seasonal variation with maximum in January, minimum in August, and maximum-minimum difference of 0.19 ng m^{-3}. *Selin et al.* [2007] used this seasonal variation as a constraint in their specification of an aqueous-phase photochemical reduction rate constant for atmospheric Hg(II), as their simulation without this reduction overestimated the seasonal amplitude (owing to photochemical Hg(0) oxidation). They did not include seasonal variation of the land source, which peaks in summer and thus compensates for the photochemical sink. Our present-day simulation including seasonal variation in the land source together with the redox chemistry of *Selin et al.* [2007] does not show a statistically significant seasonal variation in TGM at the 12 northern midlatitudes sites. This suggests that the postulated Hg(II) photochemical reduction of *Selin et al.* [2007] may be too fast. We will address this issue in future work.

6. Present-Day Enrichment Factor for Mercury Deposition

[42] Figure 6 shows the global distribution of the enrichment factor for mercury deposition, defined as the ratio of the present-day to preindustrial annual deposition flux including all deposition processes. The enrichment factor exceeds two everywhere, reflecting the global extent of anthropogenic influence. The highest enrichment factors are in anthropogenic source regions, exceeding 5 in eastern Europe and 10 in East Asia. Relatively high values in central Africa are due to artisanal mining. *Fitzgerald et al.* [1998] estimated an enrichment factor of 3.4 from lake sediment cores in Minnesota and Wisconsin; the corresponding GEOS-Chem value is 3.7. In New Zealand, GEOS-Chem reproduces the enrichment factor measured by *Lamborg et al.* [2002] (measured 3, simulated 3.1). *Lamborg et al.* [2002] report a value of 5 in Nova Scotia between preindustrial times and 1996–1999, larger than the model (3.0). Other measurements in that region show a large range of values (mean of four samples 4.3 ± 2.0) and suggest a decline in local emissions and deposition since the mid-1990s [*Sunderland and Mason*, 2008]. Higher mid-1990s

Table 1. Source Contributions in Mg a^{-1} to Mercury Deposition in the United States[a]

Source	Dry Hg(0)	Wet Hg(II)	Dry Hg(II)	Total
Natural[b]	39.0	15.4	29.3	83.7 (32%)
Anthropogenic (North America)[c]	8.5	14.0	29.9	52.4 (20%)
Primary[d]	*7.7*	*13.8*	*29.5*	*51.0*
Recycled[e]	*0.8*	*0.2*	*0.4*	*1.4*
Anthropogenic (rest of world)[c]	34.9	16.5	31.0	82.4 (31%)
Primary	*24.3*	*11.7*	*22.1*	*58.1*
Recycled	*10.6*	*4.8*	*8.9*	*24.3*
Anthropogenic (legacy)[f]	17.2	8.6	15.3	41.1 (16%)
Total	99.6	54.5	105.5	259.6 (100%)

[a]Simulated annual mean values for present day (2000) over the contiguous United States. Values for Hg(II) also include a small contribution from refractory particulate mercury (Hg(P)).

[b]Calculated from the preindustrial simulation.

[c]Determined by a sensitivity simulation shutting off the North American source (including the United States, Canada, and Mexico).

[d]The primary contribution refers to emissions not recycled through land and ocean reservoirs and is determined by a sensitivity simulation shutting off recycling.

[e]Anthropogenic emissions recycled in the model through the surface ocean and the prompt recycling mechanism for land, as determined by difference with the simulation shutting off recycling. The timescale for this recycling is of the order of 1 year (section 5.1).

[f]Legacy of anthropogenic emissions accumulated in the land and deep ocean on a centurial timescale, as determined by a simulation with anthropogenic sources shut off but including the present-day soil and deep ocean reservoirs.

emissions would not be reflected in our 2000 emissions inventory.

7. Source Apportionment for Present-Day Mercury Deposition to the United States

[43] Table 1 presents the contributions from different sources to total mercury deposition (dry + wet) in the United States, as determined from an ensemble of sensitivity simulations to isolate the contributions from individual terms. We distinguish contributions from emissions in North America versus outside, and we further distinguish (1) primary contributions not recycled through land or ocean, (2) recycled contributions having cycled through the surface ocean or the land (prompt recycling only), and (3) a legacy contribution reflecting the increased soil and deep ocean reservoirs since preindustrial times. The recycled contribution as defined in this manner involves a timescale of only $\sim$1 year for re-emission from the surface reservoirs. The legacy contribution reflects longer-term storage and recycling and is not traced in the model to a specific source region.

[44] We see from Table 1 that 68% of present-day mercury deposition in the United States is anthropogenic. This includes 20% from primary anthropogenic emissions in North America, 22% from primary anthropogenic emissions outside North America (mostly East Asia), and 26% from recycling through the land and ocean reservoirs (<1% from North America, 9% from the rest of the world, 16% from legacy). We thus find that about half of the anthropogenic enrichment of mercury deposition in the United States is due to recent emissions from outside North America, and that a quarter is due to the legacy of anthropogenic mercury accumulated in the soil and oceans since preindustrial times, leaving only a quarter that is controllable through emission reductions in North America. It should be emphasized that these are national estimates, and areas immediately downwind of major mercury sources may find greater benefits from local controls.

8. Conclusions

[45] We have developed a mechanistically based representation of the land-atmosphere cycling of mercury in a global 3-D atmospheric model (GEOS-Chem [*Selin et al.*, 2007]), complementing the previously developed ocean-atmosphere cycling in that model [*Strode et al.*, 2007]. This results in the first global 3-D atmospheric model that accounts for cycling with the surface ocean and land reservoirs and thus enables tracking of anthropogenic influence though these reservoirs. It also allows a consistent description of the mercury source from vegetation and soils based on steady state arguments for the preindustrial system. We used this model to construct and interpret the preindustrial and present-day global biogeochemical budgets and cycles of mercury. We examined the global spatial distribution of anthropogenic enrichments to mercury deposition, and more specifically the source contributions to mercury deposition in the United States.

[46] Our work included a number of updates to the GEOS-Chem ocean-atmosphere simulation originally described by *Selin et al.* [2007] and *Strode et al.* [2007]. We added an Hg(0) dry deposition sink to land, amounting to 1600 Mg a^{-1} for present day; this together with the accounting of Hg(0) uptake by the ocean results in a shorter TGM lifetime (0.50 year) than is commonly derived in models. We added mercury sources from biomass burning (600 Mg a^{-1}) and artisanal mining (450 Mg a^{-1}). Consistent with observations in Asian outflow [*Jaffe et al.*, 2005], we increased Asian anthropogenic emissions by 50% (330 Mg a^{-1}) over the 2000 GEIA emission inventory of *Pacyna et al.* [2006]. Finally, we increased GEIA anthropogenic emissions by 30% outside of Asia (300 Mg a^{-1}) in order to achieve a globally unbiased simulation of atmospheric mercury as in the work of *Selin et al.* [2007] (i.e., by balancing the new sink from Hg(0) deposition to land with new sources).

[47] Land emission processes in GEOS-Chem include prompt recycling of deposited Hg(II) (600 Mg a^{-1} for the present day), soil volatilization (550 Mg a^{-1}), and evapotranspiration (550 Mg a^{-1}). Soil volatilization is parameterized as a function of solar radiation and temperature, and both it and evapotranspiration are dependent on local soil concentrations. We derive the global distribution of soil concentrations in the preindustrial simulation by assuming local steady state between total mercury emission and deposition for land. For the present-day simulation we augment the global soil reservoir by 15% and distribute this increment according to the deposition pattern of anthropogenic mercury.

[48] Our preindustrial simulation assumes on the basis of sediment core data that mercury deposition was one-third

the present rate or 3700 Mg a^{-1}. It includes a geogenic source of 500 Mg a^{-1}, a global mean soil concentration of 43 ng g^{-1} (85% of present day), and subsurface ocean concentrations of one-third the present day. We calculate for this preindustrial simulation a net ocean evasion of 1340 Mg a^{-1} and evapotranspiration source of 500 Mg a^{-1}, and specify soil volatilization emissions (500 Mg a^{-1}) by the difference between the constrained total deposition and all other emission sources. We then determine iteratively with GEOS-Chem the distribution of soil mercury concentrations in order to enforce local steady state between deposition and land emission. Deposition is highest in the subtropics owing to subsidence of Hg(II)-enriched air, and the emissions are correspondingly high there.

[49] While our computed lifetime of mercury in the atmosphere is short (0.55 year), cycling between the atmosphere and the surface land and ocean more than doubles the effective lifetime of mercury with respect to incorporation into the long-term storage reservoirs (soils, deep ocean). For the preindustrial cycle, we find that emitted Hg(0) is transferred to the soil and deep ocean pools in a 50/50 ratio. We find that mercury released from the sediment pool, both naturally and anthropogenically (e.g., from coal combustion), has a lifetime of 3000 years in the land-ocean-atmosphere system before returning to the sediments.

[50] Our present-day global budget has a larger primary anthropogenic source (3480 Mg a^{-1}) and larger total source (11,200 Mg a^{-1}) than reported in previous literature. The larger anthropogenic source reflects our inclusion of biomass burning, artisanal mining, and upward adjustments to the GEIA anthropogenic emission inventory. The larger total source reflects in addition our accounting of gross ocean evasion (as opposed to net in the literature). Our present-day simulation has the soil reservoir increasing by 0.2% a^{-1} and the deep ocean by 0.5% a^{-1}. Both these reservoirs can be viewed as terminal sinks for mercury on a centurial timescale.

[51] Our previous GEOS-Chem model simulation [*Selin et al.*, 2007] was extensively evaluated with observations from an ensemble of surface sites and ship cruises. We examined how the changes made to the model (land cycling, anthropogenic emissions, Hg(0) deposition to land) affected its ability to fit observations. Similar to that of *Selin et al.* [2007], the model shows no global bias in the mean annual TGM concentration observed at land-based sites (1.58 ± 0.19 ng m^{-3} measured, 1.56 ± 0.09 ng m^{-3} simulated), and correlates well with wet deposition flux measurements by the U.S. Mercury Deposition Network (r^2 = 0.60 for 2003–2004). It reproduces the magnitude of total wet deposition over the U.S within 16%. However, it does not reproduce the weak but significant seasonal variation at northern midlatitudes land sites (maximum in January, minimum in August). *Selin et al.* [2007] previously reproduced this seasonal variation by photochemical oxidation of Hg(0), and needed a compensating photochemical reduction of Hg(II) to avoid overestimating the seasonal amplitude; but they did not account for the seasonal variation in land emission peaking in summer. Thus the photochemical reduction rate inferred by *Selin et al.* [2007] and used here may be excessive. We plan to address this in future work.

[52] Our simulated enrichment factors for mercury deposition from preindustrial to present day are generally consistent with data from sediment cores. The highest enrichments (5–10) are found in anthropogenic source regions, with maxima in Eastern Europe and Asia. We estimate that 68% of present-day mercury deposition to the United States is anthropogenic, of which 20% is from North American anthropogenic emissions (20% primary, <1% recycled), 31% is from anthropogenic emissions in the rest of the world (22% primary, 9% recycled), and 16% is from the legacy of anthropogenic mercury accumulated in the soil and ocean since preindustrial times.

[53] In closing, it is important to recognize that there remain at present many major uncertainties in global mercury modeling that affect our results in a manner difficult to quantify. The atmospheric Hg(0)/Hg(II) redox chemistry is poorly understood and this could have a significant effect on simulated deposition patterns. Dry deposition of Hg(0) to land, generally not included in global models, is found here to represent a major sink and hence require upward adjustment of estimated sources. Few data exist to constrain Hg(0) fluxes to land, and this represents a significant source of uncertainty regarding the total mercury budget in the model. However, the parameterization of Hg(0) deposition has little effect on surface reservoir lifetimes and enrichment factors between preindustrial and present day. Land emission of mercury has a summer maximum but atmospheric observations at northern midlatitudes show a summer minimum, suggesting the need for a faster photochemical sink for atmospheric Hg(0). The large model underestimate of atmospheric concentrations observed on ship cruises in the North Atlantic and North Pacific suggests the possibility of a large legacy of past anthropogenic emissions stored in the northern hemisphere oceans. These and other uncertainties will need to be addressed in future work.

[54] **Acknowledgments.** This work was funded by the Atmospheric Chemistry Program of the U. S. National Science Foundation and by a U. S. Environmental Protection Agency (EPA) Science to Achieve Results (STAR) Graduate Fellowship to N. E. S. Statements in this publication reflect the authors' professional views and opinions and should not be construed to represent any determination or policy of the U. S. Environmental Protection Agency.

References

Allison, J. D., and T. L. Allison (2005), Partition coefficients for metals in surface water, soil and waste, *Rep. EPA/600/R-05/074*, U.S. Environ. Prot. Agency, Off. of Res. and Dev., Washington, D.C.

Amyot, M., G. L. Southworth, S. E. Lindberg, H. Hintelmann, J. D. Lalonde, N. P. Ogrinc, A. J. Poulain, and K. A. Sandilands (2004), Formation and evasion of dissolved gaseous mercury in large enclosures amended with 200HgCl2, *Atmos. Environ.*, *38*, 4279–4289.

Andersson, A. (1967), Mercury in the soil (in Swedish), *Grundförbättring*, *20*(3–4), 95–105.

Andreae, M. O., and P. Merlet (2001), Emission of trace gases and aerosols from biomass burning, *Global Biogeochem. Cycles*, *15*, 955–966.

Andren, A., and J. O. Nriagu (1979), The global cycle of mercury, in *Biogeochemistry of Mercury in the Environment*, edited by J. O. Nriagu, Elsevier, Amsterdam.

Baker, P. G. L., E. G. Brunke, F. Slemr, and A. M. Crouch (2002), Atmospheric mercury measurements at Cape Point, South Africa, *Atmos. Environ.*, *36*, 2459–2465.

Bash, J. O., D. R. Miller, T. H. Meyer, and P. A. Bresnahan (2004), Northeast United States and Southeast Canada natural mercury emissions estimated with a surface emission model, *Atmos. Environ.*, *38*(33), 5683–5692.

Bergan, T., L. Gallardo, and H. Rodhe (1999), Mercury in the global troposphere: A three-dimensional model study, *Atmos. Environ.*, *33*, 1575–1585.

Bey, I., D. J. Jacob, R. M. Yantosca, J. A. Logan, B. D. Field, A. M. Fiore, Q. B. Li, H. G. Y. Liu, L. J. Mickley, and M. G. Schultz (2001), Global modeling of tropospheric chemistry with assimilated meteorology: Model description and evaluation, *J. Geophys. Res.*, *106*, 23,073–23,095.

Brunke, E. G., C. Labuschagne, and F. Slemr (2001), Gaseous mercury emissions from a fire in the Cape Peninsula, South Africa, during January 2000, *Geophys. Res. Lett.*, *28*, 1483–1486.

Carpi, A., and S. E. Lindberg (1998), Application of a Teflon (TM) dynamic flux chamber for quantifying soil mercury flux: Tests and results over background soil, *Atmos. Environ.*, *32*(5), 873–882.

Du, S.-H., and S. C. Fang (1982), Uptake of elemental mercury by C3 and C4 species, *Environ. Exp. Bot.*, *22*(4), 437–443.

Duncan, B. N., R. V. Martin, A. C. Staudt, R. Yevich, and J. A. Logan (2003), Interannual and seasonal variability of biomass burning emissions constrained by satellite observations, *J. Geophys. Res.*, *108*(D2), 4100, doi:10.1029/2002JD002378.

Ebinghaus, R., H. H. Kock, C. Temme, J. W. Einax, A. G. Lowe, A. Richter, J. P. Burrows, and W. H. Schroeder (2002), Antarctic springtime depletion of atmospheric mercury, *Environ. Sci. Technol.*, *36*, 1238–1244.

Ebinghaus, R., F. Slemr, C. A. M. Brenninkmeijer, P. van Velthoven, A. Zahn, M. Hermann, D. A. O'Sullivan, and D. E. Oram (2007), Emissions of gaseous mercury from biomass burning in South America in 2005 observed during CARIBIC flights, *Geophys. Res. Lett.*, *34*, L08813, doi:10.1029/2006GL028866.

Ferrari, C. P., et al. (2005), Snow-to-air exchanges of mercury in an Arctic seasonal snow pack in Ny-Alesund, Svalbard, *Atmos. Environ.*, *39*(39), 7633–7645.

Fitzgerald, W. F., and C. H. Lamborg (2005), Geochemistry of mercury in the environment, in *Treatise on Geochemistry*, vol. 9, *Environmental Geochemistry*, edited by B. S. Lollar, pp. 107–148, Elsevier, New York.

Fitzgerald, W. F., D. R. Engstrom, R. P. Mason, and E. A. Nater (1998), The case for atmospheric mercury contamination in remote areas, *Environ. Sci. Technol.*, *32*(1), 1–7.

Frescholtz, T. F., and M. S. Gustin (2004), Soil and foliar mercury emission as a function of soil concentration, *Water Air Soil Pollut.*, *155*(1–4), 223–237.

Friedli, H. R., L. F. Radke, and J. Y. Lu (2001), Mercury in smoke from biomass fires, *Geophys. Res. Lett.*, *28*, 3223–3226.

Friedli, H. R., L. F. Radke, J. Y. Lu, C. M. Banic, W. R. Leaitch, and J. I. MacPherson (2003), Mercury emissions from burning of biomass from temperate North American forests: Laboratory and airborne measurements, *Atmos. Environ.*, *37*(2), 253–267.

Gbor, P. K., D. Y. Wen, F. Meng, F. Q. Yang, B. N. Zhang, and J. J. Sloan (2006), Improved model for mercury emission, transport and deposition, *Atmos. Environ.*, *40*(5), 973–983.

Graydon, J. A., V. L. St. Louis, S. E. Lindberg, H. Hintelmann, and D. P. Krabbenhoft (2006), Investigation of mercury exchange between forest canopy vegetation and the atmosphere using a new dynamic chamber, *Environ. Sci. Technol.*, *40*(15), 4680–4688.

Grigal, D. F. (2003), Mercury sequestration in forests and peatlands: A review, *J. Environ. Qual.*, *32*(2), 393–405.

Gustin, M. S., and J. Stamenkovic (2005), Effect of watering and soil moisture on mercury emissions from soils, *Biogeochemistry*, *76*(2), 215–232.

Gustin, M. S., H. Biester, and C. S. Kim (2002), Investigation of the light-enhanced emission of mercury from naturally enriched substrates, *Atmos. Environ.*, *36*(20), 3241–3254.

Hall, B. (1995), The gas phase oxidation of elemental mercury by ozone, *Water Air Soil Pollut.*, *80*, 301–315.

Hillel, D. (1998), *Environmental Soil Physics: Fundamentals, Applications and Environmental Considerations*, Academic, San Diego, Calif.

Hintelmann, H., R. Harris, A. Heyes, J. P. Hurley, C. A. Kelly, D. P. Krabbenhoft, S. Lindberg, J. W. M. Rudd, K. J. Scott, and V. L. St. Louis (2002), Reactivity and mobility of new and old mercury deposition in a Boreal forest ecosystem during the first year of the METAALICUS study, *Environ. Sci. Technol.*, *36*(23), 5034–5040.

Holmes, C., X. Yang, and D. J. Jacob (2006), Is atomic bromine a major global oxidant of atmospheric mercury?, *Geophys. Res. Lett.*, *33*, L20808, doi:10.1029/2006GL027176.

Hylander, L. D., and M. Meili (2005), The rise and fall of mercury: Converting a resource to refuse after 500 years of mining and pollution, *Crit. Rev. Environ. Sci. Technol.*, *34*, 1–36.

Jaffe, D., E. Prestbo, P. Swartzendruber, P. Weiss-Penzias, S. Kato, A. Takami, S. Hatakeyama, and Y. Kajii (2005), Export of atmospheric mercury from Asia, *Atmos. Environ.*, *39*, 3029–3038.

Kellerhals, M., et al. (2003), Temporal and spatial variability of total gaseous mercury in Canada: Results from the Canadian Atmospheric Mercury Measurement Network (CAMNET), *Atmos. Environ.*, *37*, 1003–1011.

Kim, K. H., S. E. Lindberg, and T. P. Meyers (1995), Micrometeorological measurements of mercury-vapor fluxes over background forest soils in eastern Tennessee, *Atmos. Environ.*, *29*(2), 267–282.

Lalonde, J. D., A. M. L. Kraepiel, and F. M. M. Morel (2001), Photooxidation of Hg (0) in artificial and natural waters, *Environ. Sci. Technol.*, *35*, 1367–1372.

Lamborg, C. H., K. R. Rolfhus, W. F. Fitzgerald, and G. Kim (1999), The atmospheric cycling and air-sea exchange of mercury species in the South and equatorial Atlantic Ocean, *Deep Sea Res., Part II*, *46*, 957–977.

Lamborg, C. H., W. F. Fitzgerald, A. W. H. Damman, J. M. Benoit, P. H. Balcom, and D. R. Engstrom (2002), Modern and historic atmospheric mercury fluxes in both hemispheres: Global and regional mercury cycling implications, *Global Biogeochem. Cycles*, *16*(4), 1104, doi:10.1029/2001GB001847.

Laurier, F. J. G., R. P. Mason, L. Whalin, and S. Kato (2003), Reactive gaseous mercury formation in the North Pacific Ocean's marine boundary layer: A potential role of halogen chemistry, *J. Geophys. Res.*, *108*(D17), 4529, doi:10.1029/2003JD003625.

Lin, C.-J., and S. O. Pehkonen (1999), The chemistry of atmospheric mercury: A review, *Atmos. Environ.*, *33*(13), 2067–2079.

Lin, C. J., S. E. Lindberg, T. C. Ho, and C. Jang (2005), Development of a processor in BEIS3 for estimating vegetative mercury emission in the continental United States, *Atmos. Environ.*, *39*(39), 7529–7540.

Lin, C.-J., P. Pongprueksa, S. E. Lindberg, S. O. Pehkonen, D. Byun, and C. Jang (2006), Scientific uncertainties in atmospheric mercury models. I: Model science evaluation, *Atmos. Environ.*, *40*, 2911–2928.

Lindberg, S. E., T. P. Meyers, G. E. Taylor Jr., R. R. Turner, and W. H. Schroeder (1992), Atmosphere-surface exchange of mercury in a forest: Results of modeling and gradient approaches, *J. Geophys. Res.*, *97*, 2519–2528.

Lindberg, S. E., K. H. Kim, T. P. Meyers, and J. G. Owens (1995), Micrometeorological gradient approach for quantifying air-surface exchange of mercury vapor: Tests over contaminated soils, *Environ. Sci. Technol.*, *29*(1), 126–135.

Lindberg, S. E., P. J. Hanson, T. P. Meyers, and K.-H. Kim (1998), Air/surface exchange of mercury vapor over forests: The need for a reassessment of continental biogenic emissions, *Atmos. Environ.*, *32*(5), 895–908.

Lindberg, S. E., W. J. Dong, and T. Meyers (2002), Transpiration of gaseous elemental mercury through vegetation in a subtropical wetland in Florida, *Atmos. Environ.*, *36*(33), 5207–5219.

Lindqvist, O. (1991), Mercury in the Swedish environment: Recent research on causes, consequences and corrective methods, *Water Air Soil Pollut.*, *55*, xi–261.

Liu, H., D. J. Jacob, I. Bey, and R. M. Yantosca (2001), Constraints from 210-Pb and 7-Be on wet deposition and transport in a global three-dimensional chemical tracer model driven by assimilated meteorological fields, *J. Geophys. Res.*, *106*, 12,109–12,128.

Mason, R. P., and G.-R. Sheu (2002), Role of the ocean in the global mercury cycle, *Global Biogeochem. Cycles*, *16*(4), 1093, doi:10.1029/2001GB001440.

Mason, R. P., W. F. Fitzgerald, and F. M. M. Morel (1994), The biogeochemical cycling of elemental mercury: Anthropogenic influences, *Geochim. Cosmochim. Acta*, *58*, 3191–3198.

McElroy, M. B. (2002), *The Atmospheric Environment: Effects of Human Activity*, Princeton Univ. Press, Princeton, N.J.

Mintz, Y., and G. K. Walker (1993), Global fields of soil moisture and land surface evapotranspiration derived from observed precipitation and surface air temperature, *J. Appl. Meteorol.*, *32*(8), 1305–1334.

Myneni, R. B., R. R. Nemani, and S. W. Running (1997), Estimation of global leaf area index and absorbed PAR using radiative transfer models, *IEEE Trans. Geosci. Remote Sens.*, *35*, 1380–1393.

Nightingale, P. D., G. Malin, C. S. Law, A. J. Watson, P. S. Liss, M. I. Liddicoat, J. Boutin, and R. C. Upstill-Goddard (2000), In situ evaluation of air-sea gas exchange parameterizations using novel conservative and volatile tracers, *Global Biogeochem. Cycles*, *14*, 373–387.

Nriagu, J., and C. Becker (2003), Volcanic emissions of mercury to the atmosphere: Global and regional inventories, *Sci. Total Environ.*, *304*(1–3), 3–12.

Pacyna, E. G., J. M. Pacyna, F. Steenhuisen, and S. Wilson (2006), Global anthropogenic mercury emission inventory for 2000, *Atmos. Environ.*, *40*(22), 4048–4063.

Pal, B., and P. A. Ariya (2004), Gas-phase HO-initiated reactions of elemental mercury: Kinetics and product studies, and atmospheric implications, *Environ. Sci. Technol.*, *21*, 5555–5566.

Park, R. J., D. J. Jacob, B. D. Field, R. M. Yantosca, and M. Chin (2004), Natural and transboundary pollution influences on sulfate-nitrate-ammonium aerosols in the United States: Implications for policy, *J. Geophys. Res.*, *109*, D15204, doi:10.1029/2003JD004473.

Pirrone, N., G. J. Keeler, and J. O. Nriagu (1996), Regional differences in worldwide emissions of mercury to the atmosphere, *Atmos. Environ.*, *30*(17), 2981–2987.

Poissant, L., and A. Casimir (1998), Water-air and soil-air exchange rate of total gaseous mercury measured at background sites, *Atmos. Environ.*, *32*(5), 883–893.

Poissant, L., M. Pilote, P. Constant, C. Beauvais, H. H. Zhang, and X. H. Xu (2004), Mercury gas exchanges over selected bare soil and flooded sites in the bay St. Francois wetlands (Quebec, Canada), *Atmos. Environ.*, *38*(25), 4205–4214.

Poissant, L., M. Pilote, C. Beauvais, P. Constant, and H. H. Zhang (2005), A year of continuous measurements of three atmospheric mercury species (GEM, RGM and Hg-p) in southern Quebec, Canada, *Atmos. Environ.*, *39*, 1275–1287.

Pyle, D. M., and T. A. Mather (2003), The importance of volcanic emissions for the global atmospheric mercury cycle, *Atmos. Environ.*, *37*(36), 5115–5124.

Ravichandran, M. (2004), Interactions between mercury and dissolved organic matter: A review, *Chemosphere*, *55*, 319–331.

Richardson, G. M., I. A. Mitchell, M. Mah-Paulson, T. Hackbarth, and R. G. Garrett (2003), Natural emissions of mercury to the atmosphere in Canada, *Environ. Rev.*, *11*, 17–36.

Roos-Barraclough, F., A. Martinez-Cortizas, E. Garcia-Rodeja, and W. Shotyk (2002), A 14,500 year record of the accumulation of atmospheric mercury in peat: Volcanic signals, anthropogenic influences and a correlation to bromine accumulation, *Earth Planet. Sci. Lett.*, *202*(2), 435–451.

Schlüter, K. (2000), Review: Evaporation of mercury from soils. An integration and synthesis of current knowledge, *Environ. Geol.*, *39*(3–4), 249–271.

Seigneur, S., P. Karamchandani, K. Lohman, and K. Vijayaraghavan (2001), Multiscale modeling of the atmospheric fate and transport of mercury, *J. Geophys. Res.*, *106*, 27,795–27,809.

Selin, N. E., D. J. Jacob, R. J. Park, R. M. Yantosca, S. Strode, L. Jaeglé, and D. A. Jaffe (2007), Chemical cycling and deposition of atmospheric mercury: Global constraints from observations, *J. Geophys. Res.*, *112*, D02308, doi:10.1029/2006JD007450.

Shacklette, H. T., J. G. Boerngen, and R. L. Turner (1971), Mercury in the Environment: Surficial materials of the conterminous United States, *Geol. Surv. Circ.*, *644*, U.S. Geol. Surv., Washington, D.C.

Shia, R.-L., C. Seigneur, P. Pai, M. Ko, and N. D. Sze (1999), Global simulation of atmospheric mercury concentrations and deposition fluxes, *J. Geophys. Res.*, *104*, 23,747–23,760.

Sommar, J., K. Gårdfeldt, D. Strömberg, and X. Feng (2001), A kinetic study of the gas-phase reaction between the hydroxyl radical and atomic mercury, *Atmos. Environ.*, *35*, 3049–3054.

Strode, S., L. Jaeglé, N. E. Selin, D. J. Jacob, R. J. Park, R. M. Yantosca, R. P. Mason, and F. Slemr (2007), Air-sea exchange in the global mercury cycle, *Global Biogeochem. Cycles*, *21*, GB1017, doi:10.1029/2006GB002766.

Strode, S., L. Jaeglé, D. A. Jaffe, P. C. Swartzendruber, N. E. Selin, C. Holmes, and R. M. Yantosca (2008), Trans-Pacific transport of mercury, *J. Geophys. Res.*, doi:10.1029/2007JD009428, in press.

Sunderland, E. M., and R. P. Mason (2008), Human impacts on open ocean mercury concentrations, *Global Biogeochem. Cycles*, *21*, GB4022, doi:10.1029/2006GB002876.

Swain, E. B., P. M. Jakus, G. Rice, F. Lupi, P. A. Maxson, J. M. Pacyna, A. Penn, S. J. Spiegel, and M. M. Veiga (2007), Socioeconomic consequences of mercury use and pollution, *Ambio*, *36*(1), 45–61.

Temme, C., F. Slemr, R. Ebinghaus, and J. W. Einax (2003), Distribution of mercury over the Atlantic Ocean in 1996 and 1999–2001, *Atmos. Environ.*, *37*, 1889–1897.

Turetsky, M. R., J. W. Harden, H. R. Friedli, M. Flannigan, N. Payne, J. Crock, and L. Radke (2006), Wildfires threaten mercury stocks in northern soils, *Geophys. Res. Lett.*, *33*, L16403, doi:10.1029/2005GL025595.

Verstraete, M. M. (1987), Radiation transfer in plant canopies: Transmission of direct solar radiation and the role of leaf orientation, *J. Geophys. Res.*, *92*, 10,985–10,995.

Wang, Y., and D. J. Jacob (1998), Anthropogenic forcing on tropospheric ozone and OH since preindustrial times, *J. Geophys. Res.*, *103*, 123–131.

Wang, Y., D. J. Jacob, and J. A. Logan (1998), Global simulation of tropospheric O3-NOx-hydrocarbon chemistry: 1. Model formulation, *J. Geophys. Res.*, *103*, 10,713–10,726.

Wängberg, I., S. Schmolke, P. Schager, J. Munthe, R. Ebinghaus, and A. Iverfeldt (2001), Estimates of air-sea exchange of mercury in the Baltic Sea, *Atmos. Environ.*, *35*(32), 5477–5484.

Weiss-Penzias, P., D. A. Jaffe, A. McClintick, E. M. Prestbo, and M. S. Landis (2003), Gaseous elemental mercury in the marine boundary layer: Evidence for rapid removal in anthropogenic pollution, *Environ. Sci. Technol.*, *37*, 3755–3763.

Wesely, M. L. (1989), Parameterization of surface resistances to gaseous dry deposition in regional-scale numerical models, *Atmos. Environ.*, *23*(6), 1293–1304.

Wong, H. K. T., A. Gauthier, and J. O. Nriagu (1999), Dispersion and toxicity of metals from abandoned gold mine tailings at Goldenville, Nova Scotia, Canada, *Sci. Total Environ.*, *228*, 35–47.

Xu, X. H., X. S. Yang, D. R. Miller, J. J. Helble, and R. J. Carley (1999), Formulation of bi-directional atmosphere-surface exchanges of elemental mercury, *Atmos. Environ.*, *33*(27), 4345–4355.

Xu, X. H., X. S. Yang, D. R. Miller, J. J. Helble, and R. J. Carley (2000), A regional scale modeling study of atmospheric transport and transformation of mercury. II. Simulation results for the northeast United States, *Atmos. Environ.*, *34*(28), 4945–4955.

Zhang, H., and S. E. Lindberg (1999), Processes influencing the emission of mercury from soils: A conceptual model, *J. Geophys. Res.*, *104*, 21,889–21,896.

Zhang, H., S. E. Lindberg, F. J. Marsik, and G. J. Keeler (2001), Mercury air/surface exchange kinetics of background soils of the Tahquamenon River watershed in the Michigan Upper Peninsula, *Water Air Soil Pollut.*, *126*(1–2), 151–169.

D. J. Jacob and R. M. Yantosca, Department of Earth and Planetary Sciences, Harvard University, Cambridge, MA 02138, USA.

L. Jaeglé and S. Strode, Department of Atmospheric Sciences, University of Washington, Seattle, WA 98195, USA.

N. E. Selin, Joint Program on the Science and Policy of Global Change and Center for Global Change Science, Department of Earth, Atmospheric and Planetary Sciences, Massachusetts Institute of Technology, 77 Massachusetts Avenue, Building 54-1715, Cambridge, MA 02139-4307, USA. (selin@mit.edu)

E. M. Sunderland, U.S. Environmental Protection Agency, Washington, DC 20460, USA.